Journal of Volcanology and Geothermal Research, 30 (1986)1—27
Elsevier Science Publishers B.V., Amsterdam — Printed in The Netherlands

PETROLOGY OF MATTHEW AND HUNTER VOLCANOES, SOUTH NEW HEBRIDES ISLAND ARC (SOUTHWEST PACIFIC)

PATRICK MAILLET[1], MICHEL MONZIER[1] and CHRISTIAN LEFEVRE[2]

[1] *Centre ORSTOM, BP A5, Nouméa-Cedex, Nouvelle-Calédonie*
[2] *Laboratoire de Pétrologie, Sciences de la Terre, Bât. SN5, Université des Sciences et Techniques de Lille, 59655 Villeneuve d'Ascq-Cedex, France*

(Received July 18, 1985; revised and accepted April 14, 1986)

ABSTRACT

Maillet, P., Monzier, M. and Lefèfre, C., 1986. Petrology of Matthew and Hunter volcanoes, south New Hebrides island arc (southwest Pacific). *J. Volcanol. Geotherm. Res.*, 30: 1—27.

Matthew and Hunter, the two southernmost active volcanoes of the New Hebrides island arc (southwest Pacific) differ markedly from the other (mainly tholeiitic Quaternary volcanoes of this arc.

Geodynamically related to the New Hebrides subduction zone, they also lie close to the southern limb of the active expanding ridge of the North Fiji Basin. Both volcanoes are made up of acid, medium-K, calcalkaline orogenic andesites, containing a variety of inclusions (pyroxene- and gabbroic cumulates, as well as doleritic cognate inclusions). This paper presents the first systematic petrographic and chemical study of these volcanics and their inclusions.

Trace-element geochemistry and rare-earth element modelling suggest that the two volcanoes developed from successive batches of similar parental magmas, originating from limited partial fusion of garnet peridotite in the mantle wedge. Various degrees of fractional crystallization of these batches led to the formation of three volcanic suites: Hunter (little fractionated), West-Matthew (moderately fractionated) and East-Matthew (highly fractionated). Moreover, on Matthew island, no correlation exists between the degree of fractionation and the eruptive chronology, the youngest edifice (West-Matthew) being less evolved than the older one (East-Matthew).

INTRODUCTION

Although subduction is generally accepted as the primary cause and necessary condition for the predominance of orogenic andesites in island arcs (Gill, 1981; Thorpe, 1982), the precise role of subducted ocean crust and/or overlying upper mantle wedge in producing the geochemical patterns of andesitic volcanism remains to be ascertained. Moreover, theoretical difficulties complicate dealing with transition zones between normal convergent plate boundaries and transform fault areas. An example of such a complex zone can be found along the southern edge of the New Hebrides

0377-0273/86/$03.50

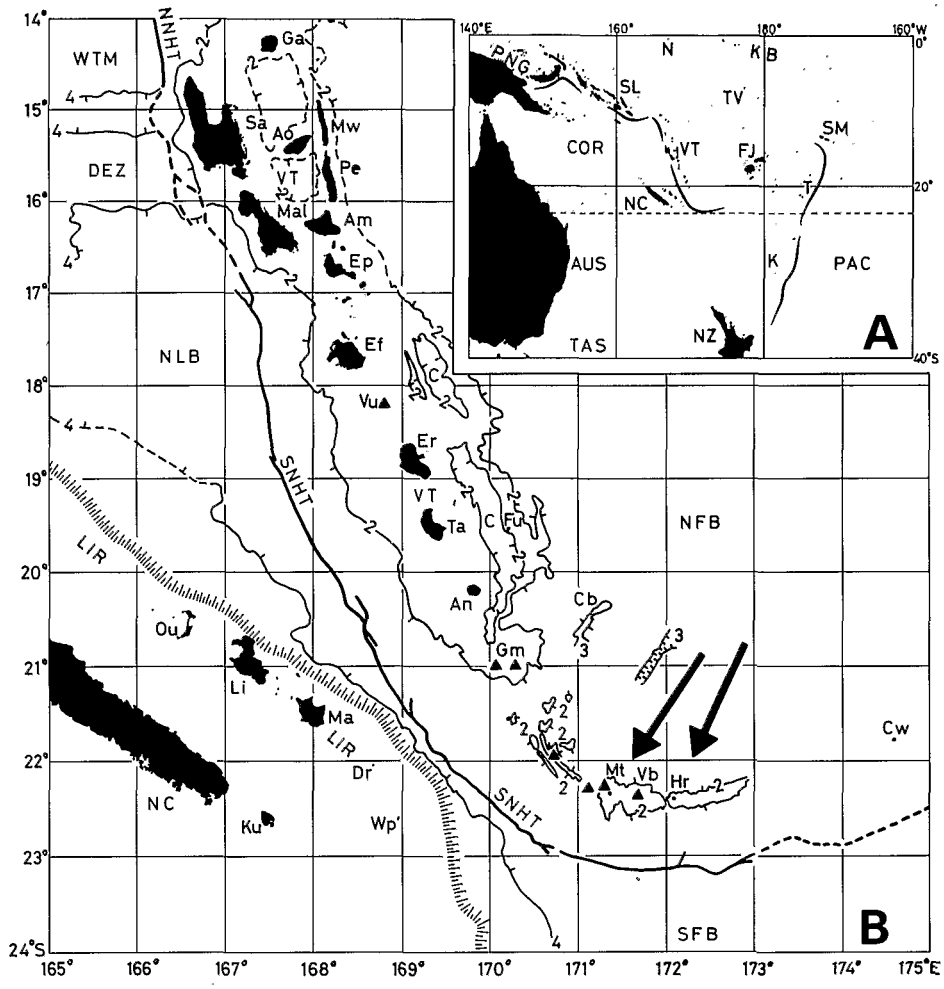

Fig. 1. Map of the southwestern Pacific (A) and outline map of the Vanuatu-New Caledonia region (B), showing major physiographic features and location of Matthew and Hunter volcanoes (arrows).

A: *PAC* = Pacific Ocean; *COR* = Coral Sea; *TAS* = Tasman Sea; *AUS* = Australia; *PNG* = Papua New Guinea; *N* = Nauru; *SL* = Solomon Islands; *VT* = Vanuatu; *NC* = New Caledonia; *NZ* = New Zealand; *K* = Kermadec Islands; *T* = Tonga Islands; *FJ* = Fiji Islands; *SM* = Samoa Islands; *TV* = Tuvalu; *KB* = Kiribati.

B: Generalized bathymetry (in km) from Monzier et al. (1984b), modified around Matthew and Hunter islands; *VT* = Vanuatu; *NC* = New Caledonia; *NFB* = North Fiji Basin; *C* = Coriolis Troughs; *SFB* = South Fiji Basin; *LIR* = Loyalty Islands Ridge (the hatched line marks the eastern scarp of this ridge); *NLB* = North Loyalty Basin; *DEZ* = D'Entrecasteaux Zone; *WTM* = West Torres Massif; *NNHT* = Northern New Hebrides Trench; *SNHT* = Southern New Hebrides Trench; *Ku* = Kunie (Pines Island); *Ou* = Ouvea; *Li* = Lifou; *Ma* = Maré; *Dr* = Durand Reef; *Wp* = Walpole; *Ga* = Gaua; *Sa* = Santo; *Mw* = Maewo; *Ao* = Aoba; *Pe* = Pentecost; *Mal* = Malekula; *Am* = Ambrym; *Ep* = Epi; *Ef* = Efate; *Vu* = Vulcan Seamount; *Er* = Erromango; *Ta* = Tanna; *Fu* = Futuna; *An* = Aneityum; *Cb* = Constantine Bank; *Gm* = Gemini Seamounts; *Mt* = Matthew; *Vb* = Vauban Seamount; *Hr* = Hunter; *Cw* = Conway (Theva-i-ra).

island arc, southwest Pacific; Matthew and Hunter are the two southernmost active volcanoes of this arc (Fig. 1).

Previous geological and petrological studies of the New Hebrides island arc (e.g. Gorton, 1977; Roca, 1978; Coulon and Maury, 1981; Barsdell et al., 1982; Dupuy et al., 1982; Carney and Macfarlane, 1982; Marcelot et al., 1983) drew attention to the characteristics of this active intra-oceanic subduction zone. Among them, the most striking features of the Quaternary–Recent volcanism can be summarized as following:

— Notwithstanding the remark of Arculus (1981, p. 118) about the difficulty of estimating the bulk petrographic composition of an arc, basalts and basaltic andesites represent the predominant rock type, whereas andesites and more felsic volcanics are subordinate. Most of the recent volcanics can be related to the island-arc tholeiitic rock series.

— Although no clear across-strike arc variations appear in magma composition, subduction of the aseismic D'Entrecasteaux Zone in the central part of the arc (Fig. 1) seems to be responsible for some along-strike arc structural (Collot et al., 1985), mineralogical, geochemical (Roca, 1978), and isotopic (Briqueu and Lancelot, 1983) variations, i.e. the so-called 'edge-effects' of Gill (1981).

We present in this paper some new petrological data relating to the andesites from Matthew and Hunter islands and discuss their relationships and petrogenetic implications.

PETROLOGY OF MATTHEW AND HUNTER VOLCANOES

Tectonic setting

The volcanoes Matthew and Hunter mark the southeasternmost tip of the Quaternary volcanic chain of the New Hebrides island arc (Fig. 2; Daniel et al., 1982; Louat, 1982). They also lie close to the southern limb of the actively spreading ridge of the North Fiji Basin. Precise location, orientation and opening rate of this spreading system are still somewhat conjectural (Fig. 3).

According to the model of Monzier et al. (1984a), the length of the slab underthrusting Matthew and Hunter volcanoes remains constant (ca. 220 km) between 21.5°S and 23°S. However, its dip decreases southward, because two hinge zones are tearing the downgoing plate. The slab lies at a depth of about 85 km beneath both volcanoes.

Because the slip-vectors for underthrusting earthquake solutions remain almost perpendicular to the trench in the entire southern New Hebrides arc (Fig. 2C), a combination of strike-slip and normal subduction movements seems preferable over oblique subduction in this area (Fitch, 1972; Beck, 1983). Accordingly, a fault complex, equivalent to a sinistral shear, would affect the Matthew-Hunter volcanic chain, as schematically shown in Fig. 3. Topographic features (Fig. 2A) and focal mechanisms (Fig. 2C)

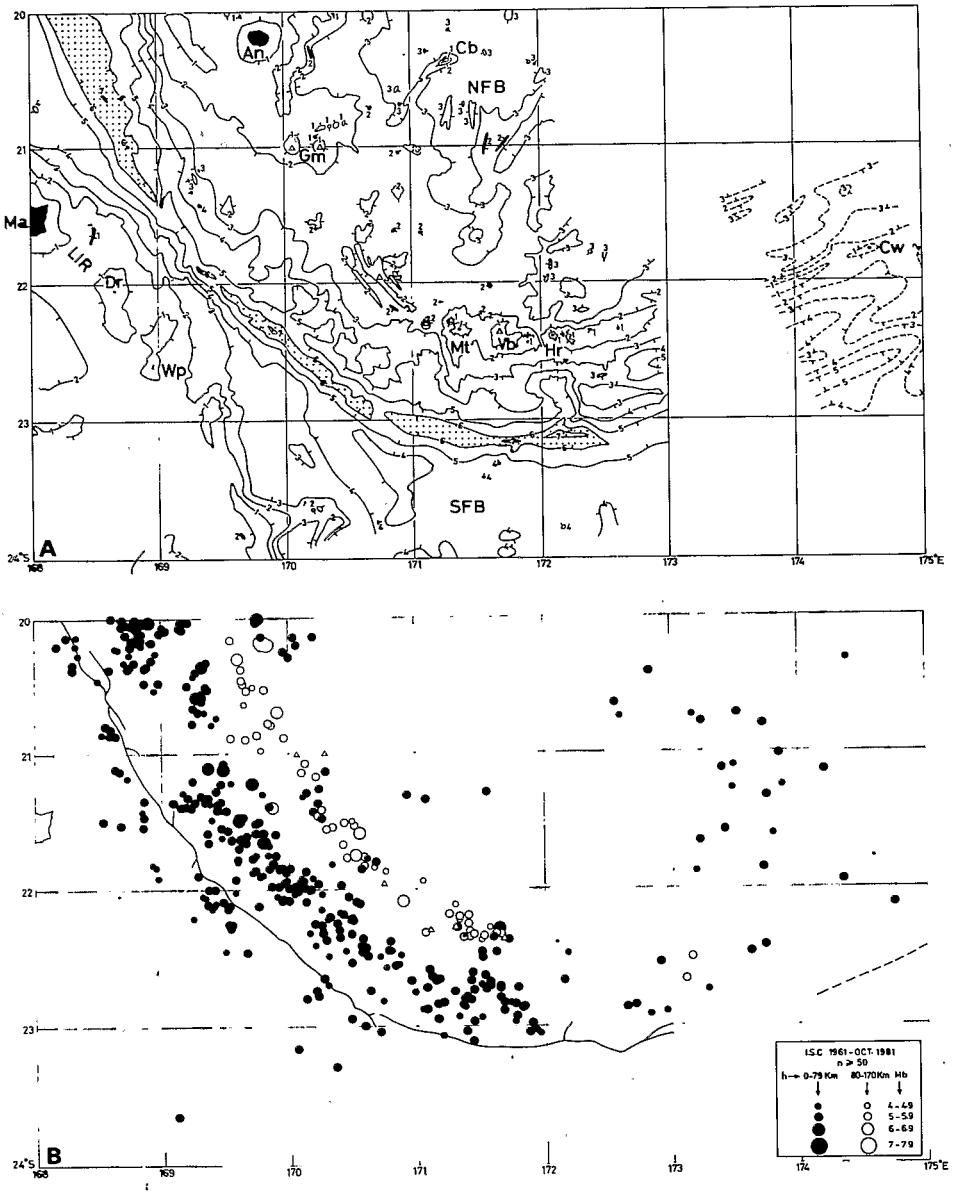

Fig. 2. Tectonic setting of Matthew and Hunter volcanoes (southern New Hebrides island arc and related areas).

A. Bathymetry (in km) from Monzier et al. (1984b), modified around Matthew and Hunter islands and augmented by Halunen's (1979) bathymetric data, eastward of 173°E; tickmarks point towards lows; abbreviated toponymy from Fig. 1B.

B. Spatial distribution of shallow (0—79 km: solid circles) and intermediate (80—170 km: open circles) focus earthquakes (International Seismological Centre catalogue from 1961 to october 1981).

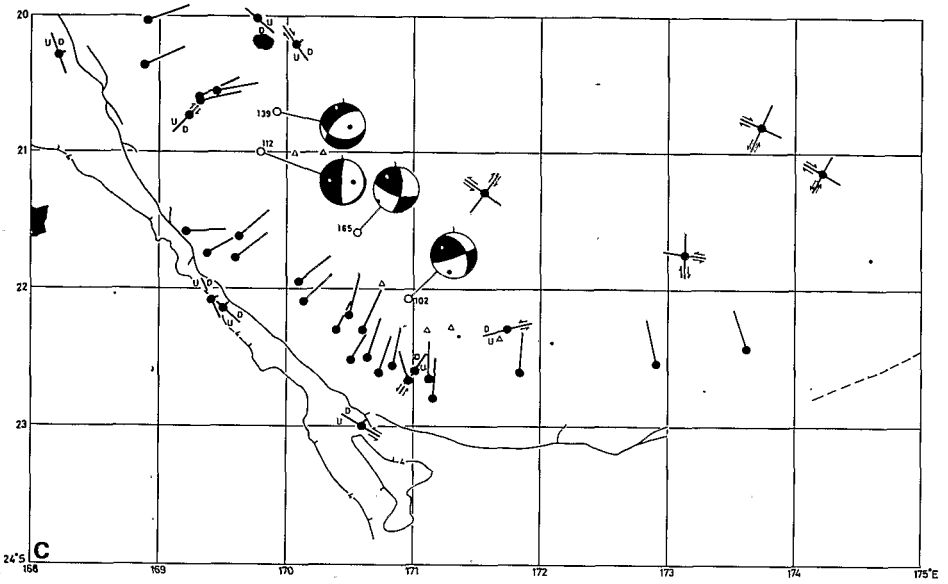

Fig. 2. C. Focal mechanism solutions for shallow and intermediate earthquakes (data from Sykes et al., 1969; Isacks and Molnar, 1971; Johnson and Molnar, 1972; Pascal et al., 1978; Coudert et al., 1981; USGS/NEIS, Preliminary Determination of Epicenters, monthly listing, February 1981 to August 1983; Vidale and Kanamori, 1983). Slip vectors of shallow underthrust mechanisms shown as single lines. Single preferred plane or both planes of shallow normal fault, strike-slip and vertical dip-slip solutions shown as lines with arrows and *U* (Up) and *D* (Down) symbols indicating sense of movement. Focal mechanism solutions of intermediate earthquakes shown as lower hemisphere projections, with focus depths in kilometers.

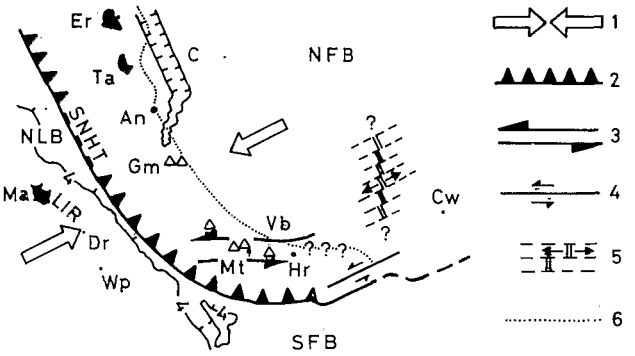

Fig. 3. Schematic model for the termination of the southern New Hebrides subduction zone (abbreviated toponymy from Fig. 1—B). *1* = Relative convergent motion between the India-Australia plate and the New Hebrides microplate (Dubois et al., 1977; Coudert et al., 1981; Isacks et al., 1981). *2* = Active convergence. *3* = Matthew-Vauban-Hunter ridge: a complex faulted zone (conjugate dextral N 160—165 E and sinistral N 70—75 E strike-slip faults: unpublished data) equivalent to a sinistral shear (Fitch, 1972; Beck, 1983). *4* = Active transform fault. *5* = Active spreading center (strikes of spreading axis and transform faults are hypothetical). *6* = Approximate projection of the eastern boundary of the intermediate seismicity (Louat et al., in press).

permit such an interpretation. Finally, south of 21.5°S, the impingement of the Loyalty Islands Ridge on the trench begins to disturb the subduction regime.

Geology

Preliminary reports about the petrology of Matthew and Hunter islands have already been published (Fisher, 1957; Curtis, 1962; Rémy, 1963; Maillet and Gill, 1980; Maillet and Monzier, 1982; Maillet et al., 1982; Lefèvre et al., 1982). Both volcanic islands are in the solfataric stage and represent the very upper part of similar-scale submarine edifices (approximate total volume for each one: 12—15 km^3). They are aligned along a 1000—1500-m-deep, easterly trending ridge (the Matthew-Hunter ridge), at a distance of about 85 km from the trench (Fig. 2A).

Matthew island (Fig. 4) is built up by two distinct prominences (East-Matthew and West-Matthew) separated by an isthmus (Priam, 1962, 1964). East-Matthew is a half-destroyed composite volcanic cone, composed of at least 3 subhorizontal, 15—30-m-thick, superimposed lava flows, displaying columnar jointing. These flows are cut by numerous subvertical N—S oriented, meter-thick feeder dykes. Thin pyroclastic formations crop out in the southern part of East-Matthew. Two basal scarps, 20—25 m high, with distinct columnar jointing structure, mark the eastern limit of the isthmus. They probably expose the oldest part of the East-Matthew cone.

West-Matthew is a roughly circular volcano composed almost wholly of lava flows. Its central crater is occupied by a spectacular, ca. 20-m-thick, NW-trending aa-flow. A lateral vent sharply cuts the eastern flank of the cone along a radial fracture, exposing E—W dykes and lava flows in ca. 50-m-high cliffs. Strongly active fumaroles and solfataras occur in a gorge which rings the southern peak. The latter may represent remainders of a Peléean-type eruption (Priam, 1964).

Only East-Matthew existed when Captain Thomas Gilbert discovered the island in 1788 (Priam, 1964). West-Matthew appeared in the late 1940's (Taylor, 1956; Koch, 1958; Priam, 1962, 1964; Simkin et al., 1981), after a highly seismically active period (Blot, 1976).

Fig. 4. Matthew island (outlines from vertical aerial photographs taken in June 1979). A. Major physiographic features and toponymy: *I* = East-Matthew; *II* = isthmus (stippled); *III* = West-Matthew; *1* = eastern peak; *2*, *3*, *4* = upper, middle and lower lava flows; *5*, *6* = northern and southern basal scarps; *7* = automatic meteorological station; *8*, *9* = northern and southern bay; *10* = radial gorge; *11* = lateral vent; *12* = U-shaped central crater rim; *13* = U-shaped gorge; *14* = central crater; *15* = NW-trending aa-lava flow; *16* = main volcanic graben; *17* = youngest lateral vents; *18* = volcanic graben; *19* = southern peak. Estimated altitudes in meters.
B. Main faults, fractures and dykes (*d*); fumarolic and solfataric areas (asterisks) whose temperatures were measured in December 1979.
C. Sample localities; *35*, *39*, *40* = systematic inclusion sampling areas.

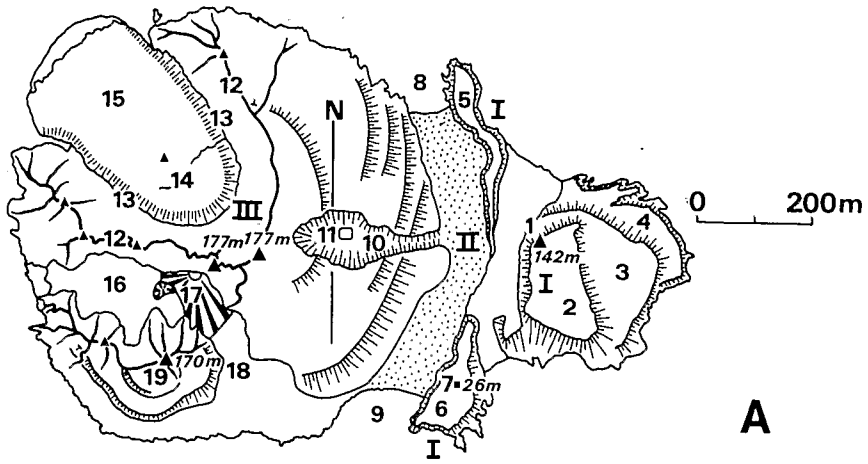
N
0
200m
15
12
13
14
13
III
12
177m
177m
11
10
8
5
I
II
1
4
142m
I
3
2
16
17
19
170m
18
7
26m
9
6
I
A

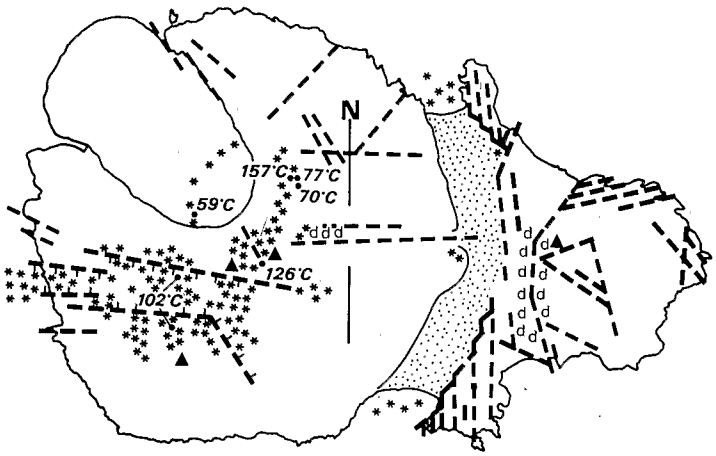
N
157°C
77°C
70°C
59°C
126°C
102°C
B

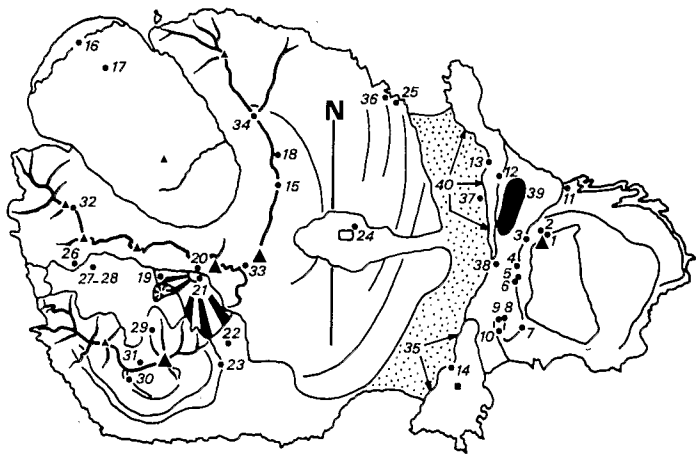
N
16
17
34
18
15
36
25
32
26
27,28
19
20
21
33
24
13
12
40
37
39
11
2
1
3
4
5
6
38
9
8
10
7
29
31
30
22
23
35
14
C

Following a cone-building stage, directed blasts partly destroyed the edifice. The northwestern lava flow then was erupted, as violent gas emissions from the lateral vent tore the eastern part of the cone. The volcanic activity moved southwards and included the extrusion of a possible spine (southern peak). An active vent was observed in 1954 in the same area, and volcanic grabens opened between 1954 and 1958. No noticeable eruptive event nor change in island morphology has occurred since 1958.

Hunter island (Fig. 5) presents an asymmetrical morphology: the southern composite cone, centered around an extinct crater, drastically differs from the northwestern part of the island, where steep cliffs, more than 100 m high in places, enclose an explosion crater. These cliffs expose outcrops of massive lavas, displaying columnar jointing. The summit of Hunter volcano presumably is formed by a Peléean-type dome. The most recent

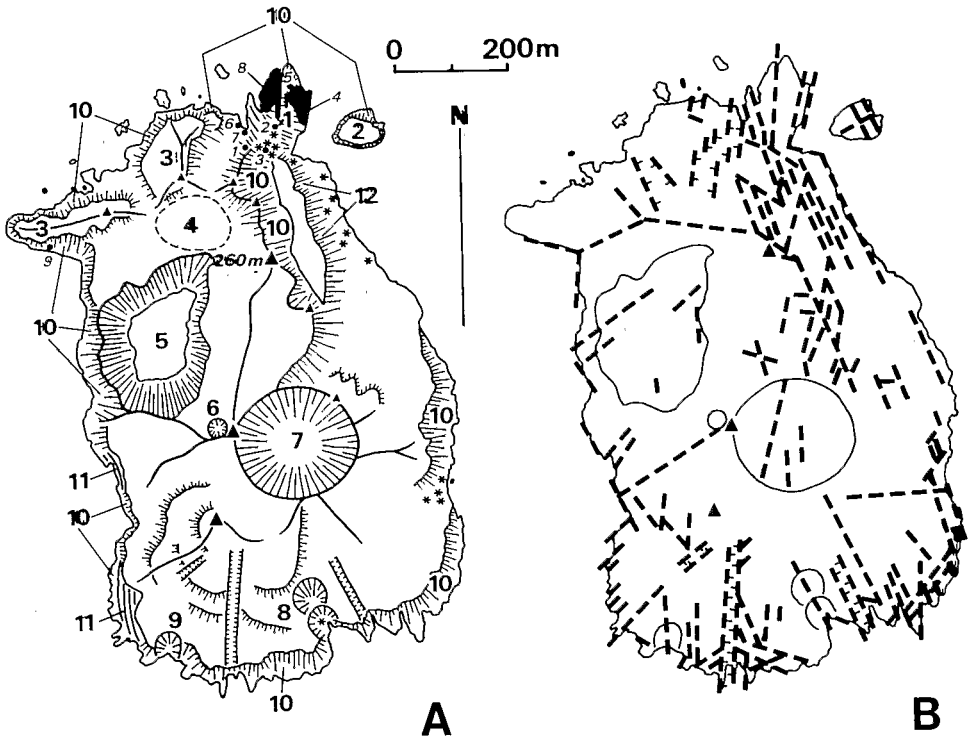

Fig. 5. Hunter island (outlines from vertical aerial photographs taken in June 1979). A. Major physiographic features, toponymy, fumarolic and solfataric areas (asterisks), and sample localities (small numbers); *1* = recent northern lava flow; *2* = islet; *3* = old lava flows; *4* = possible locality of an old crater; *5* = deep explosion crater; *6* = small crater; *7* = central crater of the southern composite cone; *8*, *9* = lateral vents; *10* = lava cliffs displaying columnar jointing; *11* = pyroclastic formations; *12* = cliff of altered lava. Estimated altitude in meters. Sample localities *4* and *8* = systematic inclusion sampling areas.
B. Main faults and fractures.

volcanic event apparently took place at the very northern point of the island, where a narrow lava flow extruded, along a major subvertical fault. Solfatara fields are common in this area.

Petrography and mineralogy

As mentioned in previous studies (Maillet and Gill, 1980; Maillet and Monzier, 1982), there is no essential difference in petrography and major-element geochemistry between the volcanic rocks of Matthew and Hunter. Both volcanoes are made up of highly porphyritic, inclusion-rich, two-pyroxene andesites. According to Gill's (1981) classification, these volcanics are calc-alkaline, high-silica, medium-K orogenic andesites. They contain three main kinds of inclusions: doleritic cognate inclusions, gabbroic- and pyroxene cumulates.

The lavas

Phenocryst assemblages, in decreasing proportions, are plagioclase feldspar (PLAG), clinopyroxene (CPX), orthopyroxene (OPX), titano-magnetite (Fe-Ti OX) and olivine (OL)/olivine and titanomagnetite for Hunter (Tables 1 and 2). These mineral phases, except for olivine, appear in the typically silica-rich (tridymite) matrix. Glomeroporphyritic clusters (PLAG+ CPX+ OPX+Fe-Ti OX) are frequent, as often noticed in orogenic andesites (Gill, 1981).

The following crystallization path can be deduced from petrographic examination of textural relationships. Initially, olivine (and, to a lesser extent, clinopyroxene) is a liquidus phase. The progressive resorption of olivine accompanies the formation of titano-magnetite and orthopyroxene, which crystallize together with calcic plagioclase and clinopyroxene. Some pyroxene-rich glomeroporphyritic clusters also may form during this stage. Subsequently, massive crystallization of labradorite occurs, while formation of pyroxenes and titano-magnetite continues. Eruption interrupts this evolution. Pyroxene, plagioclase and opaque microlites crystallize in a chilled, silica-rich matrix (tridymite filling vesicles). Post-eruption stage is represented by secondary minerals deposited around fumaroles (hematite, sulphur, silica, halite, gypsum . . .).

The early separation of titano-magnetite from the melt presumably indicates a rather high f_{O_2} (Osborn, 1962). Similarly, P_{H_2O} in the magma was important, since pyroxenes crystallized prior to plagioclases (Nesbitt and Hamilton, 1970; Green, 1972).

Modal analyses generally indicate a high phenocryst content (27—46% in vol.), ranging from East-Matthew (27—38%) to West-Matthew (37—46%), with Hunter (32—43%) intermediate (Fig. 6A). The phenocryst content is largely determined by plagioclase content, and, to a lesser extent, by pyroxene content, the sum (PLAG+CPX+OPX) in vol.% accounting for ca. 95% of the total phenocryst content for both volcanoes. Such modal

TABLE 1

Chemical analyses (major and trace elements) and modal analyses of selected lavas from East-Matthew, West-Matthew and Hunter

		EAST-MATTHEW (= OLD MATTHEW)					WEST-MATTHEW (= NEW MATTHEW)					HUNTER			
		MT 1C	MT 7B	MT11A	MT13A	MT14B	MT16B	MT 20	MT23B	MT24A	MT24C	HR 1	HR 4B	HR 6	HR 9
SiO_2		60.3	59.5	60.8	60.2	59.9	62.1	62.8	61.4	61.0	62.0	61.5	61.1	61.0	61.9
TiO_2		0.45	0.45	0.42	0.42	0.42	0.40	0.38	0.38	0.41	0.43	0.36	0.37	0.36	0.37
Al_2O_3		16.6	16.4	16.1	16.6	16.3	16.7	16.8	16.7	16.2	16.0	15.9	15.7	15.9	16.2
Fe_2O_3*		6.3	6.5	6.3	6.3	6.4	5.8	5.0	5.6	6.2	6.1	5.9	6.2	6.2	5.7
MnO		0.10	0.10	0.10	0.10	0.09	0.07	0.07	0.10	0.11	0.10	0.12	0.11	0.12	0.11
MgO		3.6	3.9	4.1	3.8	4.1	2.8	2.3	3.2	3.9	3.9	4.2	5.5	4.8	4.2
CaO		6.9	7.2	7.0	7.2	7.4	6.2	6.1	6.5	6.8	6.7	6.6	6.5	6.5	6.7
Na_2O		3.9	3.8	3.9	3.8	3.8	4.4	4.3	4.2	4.0	3.9	4.0	3.8	3.7	3.9
K_2O		1.0	0.9	0.9	1.0	1.0	1.0	1.0	0.9	0.9	0.9	1.0	0.9	0.8	0.9
LOI		0.0	0.1	0.0	0.0	0.0	0.4	0.1	0.2	0.0	0.1	0.0	0.0	0.1	0.0
TOTAL		99.15	98.85	99.62	99.42	99.41	99.87	98.85	99.18	99.52	100.13	99.58	100.18	99.48	99.98
FeO		3.8	3.8	3.5	3.1	3.5	2.1	2.7	3.1	3.7	3.3	3.9	5.0	4.2	3.9
P_2O_5	CAESS	0.18	0.18	0.17	0.18	0.18	0.13	0.13	0.13	0.14	0.13	0.13	0.13	0.12	
	UCSC	0.16		0.15		0.16	0.12	0.12	0.13		0.12		0.11		0.11
Rb	CAESS	13	14	13	12	12		13	11	12	13	19	17	15	
	UCSC	12		13		14	13	15	12		11		18		19
	P.SUE	10.1		8.6		11.7		12.6	9.3		7.6	13.9	16.5	12.3	18
Sr	CAESS	721	748	650	718	723		490	505	497	486	348	353	343	
	UCSC	714		668		732	487	481	490		469		358		376
	P.SUE	753		676		703		494	380		433	215		225	
Ba	P.SUE	152		139		140		139	118		91	123	123	100	128
Zr	CAESS	98	97	96	99	92		100	83	86	87	79	76	76	
	UCSC	112		107		110	99	108	96		89		81		88
	P.SUE					57			74						
Y	CAESS	13	13	12	12	12		14	13	13	12	10	12	12	
	UCSC	14		14		15	14	15	14		13		13		13
Nb	CAESS	<10	<10	12	<10	<10		<10	<10.	<10	<10	33	11	18	
	UCSC	11		12		9	10	11	8		8		13		12
Th	P.SUE	1.65		1.53		1.74		1.16	1.06		1.01	0.85	0.89	0.81	0.88
U	P.SUE	0.59		0.63		0.64		0.44	0.43		0.56	0.42	0.41	0.35	0.51
La	P.SUE	12.5		12.3		13.2		9.3	8.6		7.8	5.4	6.6	6.3	6.2
Ce	P.SUE	24.4		27.6		27.8		17.1	18.8		14.7	12.4	12.7	13.7	13.2
Sm	P.SUE	3.04		2.92		3.01		2.40	2.24		1.75	1.69	1.87	1.64	1.84
Eu	P.SUE	1.08		0.97		1.12		0.88	0.66		1.18	0.82	0.79	0.72	0.79
Tb	P.SUE	0.32		0.31		0.33		0.30	0.32		0.29	0.22	0.26	0.25	0.25
Yb	P.SUE	1.02		0.84		0.78		1.08	0.86		0.99	0.72	0.64	0.64	0.93
Lu	P.SUE	0.24		0.20		0.20		0.18	0.17		0.20	0.16	0.17		0.13
Ni	CAESS	22	20	30	27	26	16	17	22	27	27	32	75	39	
	UCSC	18		30		26	17	15	23		26		90		37
	P.SUE	12.5		30		29		14.5	23		27	36	89	47	36
Cr	CAESS	31	41	91	73	57	31	30	67	72	78	109	244	128	
	P.SUE	52.7		94		72		45	77		80	118	236	161	129
V	CAESS	166	158	151	154	148	116	135	112	145	140	169	156	182	
Sc	P.SUE	20.1		21.1		22.3		15.4	19.1		20.3	21.9	19.6	22.5	19.5
Cs	P.SUE					0.05		0.20	0.15		0.12	0.13	0.14		0.21
Sb	P.SUE	0.10		0.10		0.07					0.07	0.23	0.18		0.23
Zn	P.SUE	37.4						34					25		25
MODAL PHENOCRYST MINERALOGY (Vol. %)															
Plagioclase		22.7	19.5	21.3	21.9	20.6	29.2	32.8	22.4	28.8	28.1	24.4	22.6	18.3	22.5
Clinopyroxene		5.6	4.9	6.3	7.8	7.2	3.6	6.6	9.7	5.9	7.7	8.1	7.9	7.1	5.9
Orthopyroxene		4.5	3.6	3.9	3.8	3.5	3.7	5.1	4.1	4.2	3.8	4.2	5.7	4.7	5.4
Fe-Ti Oxides		0.9	0.8	1.0	1.1	1.0	1.1	1.2	1.0	0.8	0.7	0.6	0.5	0.6	0.5
Olivine		0.2	0.0	0.3	0.9	0.2	0.1	0.0	0.1	0.6	1.2	0.9	1.7	1.6	0.7
TOTAL		33.9	28.8	32.8	35.5	32.5	37.7	45.7	37.3	40.3	41.5	38.2	38.4	32.3	35.0

Source of data and analytical procedures:
(a) major elements (wt.%): ORSTOM-Nouméa (analysts: D. Duhet and S. Le Corvaisier). Analytical procedure: the samples are fused with Sr-metaborate, then analyzed by automatic colorimetry for Si, Al, Fe, Ti; by atomic absorption spectrometry for Mg, Ca, Mn, Na; by flame-emission spectrometry for K. Fe_2O_3* = total iron as Fe^{3+}. FeO = ferrous iron analyzed separately, by colorimetry. P_2O_5 = X-ray fluorescence (CAESS, UCSC; see below).
(b) trace elements (ppm): *CAESS* (Centre Armoricain d'Etude Structurale des Socles, Institut de Géologie, Université de Rennes, France): X-ray fluorescence; analyst: F. Vidal. *UCSC* (University of California, Santa Cruz, U.S.A.): X-ray fluorescence; analyst: P. Maillet. *P. SUE* (Groupe des Sciences de la Terre, Laboratoire Pierre SUE, C.E.N. Saclay, France: neutron-activation analysis; principal analyst: G. Meyer.
(c) modal phenocryst mineralogy based on more than 3000 points.

TABLE 2

Mean compositions and standard deviations for major-element analyses of Matthew and Hunter lavas

	EAST-MATTHEW (= OLD MATTHEW)		WEST MATTHEW (= NEW MATTHEW)		HUNTER	
	$\bar{x}$ (20)	s	$\bar{x}$ (15)	s	$\bar{x}$ (7)	s
SiO_2	60.16	0.65	62.03	1.16	60.90	0.66
TiO_2	0.45	0.02	0.41	0.02	0.37	0.01
Al_2O_3	16.27	0.29	16.46	0.35	15.93	0.16
Fe_2O_3*	6.37	0.20	5.76	0.41	6.03	0.18
MnO	0.11	0.01	0.09	0.02	0.11	0.01
MgO	3.91	0.36	3.23	0 65	4.91	0.53
CaO	7.02	0.25	6.39	0.44	6.67	0.15
Na_2O	3.84	0.09	4.16	0.17	3.84	0.10
K_2O	0.92	0.04	0.91	0.09	0.89	0.07
LOI	0.04	0.05	0.12	0.14	0.03	0.05
TOTAL	99.09		99.56		99.68	
FeO	3.53	0.23	3.11	0.60	4.34	0.54
P_2O_5 (CAESS and UCSC)	0.17 (8)	0.01	0.13 (12)	0.01	0.13 (7)	0.01
MODAL PHENOCRYST	MINERALOGY (vol.%)					
Plagioclase	22.26	2.98	28.58	3.49	23.07	2.95
Clinopyroxene	6.09	1.16	6.79	1.53	7.16	0.80
Orthopyroxene	3.97	0.50	4.29	0.51	4.99	0.56
Fe-Ti Oxides	0.92	0.20	1.01	0.24	0.49	0.11
Olivine	0.43	0.52	0.37	0.36	1.77	1.06
TOTAL	33.67		41.04		37.48	
Bulk Density	2.70 (18)	0.04	2.58 (14)	0.08	2.79 (7)	0.05

Source of data: Table 1 and unpublished data. Complete data available upon request (P.M.). $\bar{x}$ = mean; (20) = number of analyses; s = standard deviation.

characteristics are common in intermediate volcanics of the island-arc series (Ewart, 1976, 1982).

Calculated liquid compositions based on phenocryst mineralogy (Lefèvre et al., in press) and whole-rock modal analyses also range from East-Matthew (SiO_2=66.8%) to West-Matthew (SiO_2=71.0%) with Hunter (SiO_2=67.4%) intermediate. The positive correlations between PLAG, whole-rock SiO_2 and Al_2O_3 (Figs. 6B, 7; and Ewart, 1976) as well as the preceding observations show that plagioclase accumulation occurred (at least for Matthew volcanics) within the magmatic chamber, together with a silica-enrichment of the residual melt.

Detailed microprobe mineralogy of Matthew and Hunter andesites and their inclusions is published elsewhere (Lefèvre et al., in press). To summarize (also see Table 3).

Plagioclase. Phenocryst compositions range from An_{69} to An_{45}. Normal zoning is common. Labradorite is the predominant plagioclase in lavas of both volcanoes. Microlite compositions (An_{64-50}) are similar to those of phenocrysts.

Clinopyroxene. In general, the phenocrysts have diopside-endiopside cores and salite to augite rims. Groundmass clinopyroxenes are Ca-depleted (augite-subcalcic augite).

Orthopyroxene. The range of orthopyroxene compositions (Fs_{27-34}) is

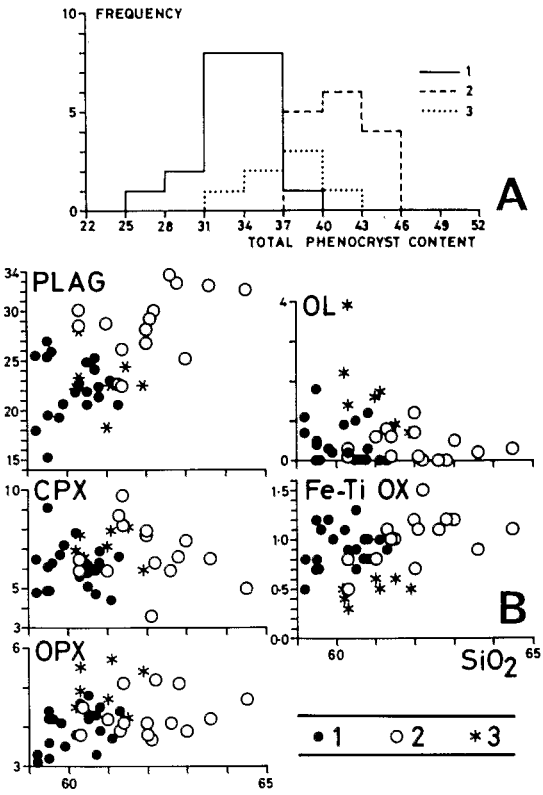

Fig. 6. A. Histogram showing the distribution of total phenocryst contents (vol. %) of lavas from East-Matthew (*1*), West-Matthew (*2*) and Hunter (*3*). B. Phenocryst contents (vol. %) plotted against SiO_2 for the lavas of East-Matthew (*1*), West-Matthew (*2*) and Hunter (*3*). Source of data: Table 1 and unpublished data. Complete analytical data available upon request (P.M.).

very narrow and falls within the bronzite-hypersthene limit. Groundmass minerals in Hunter may have more Mg-rich compositions (Fs_{17-30}), whereas in Matthew they have more Fe-rich compositions (Fs_{33-35}).

Olivine. Andesites from Matthew island contain olivine that is significantly Mg-rich (Fo_{82-88}) in comparison with usual medium-K lavas (Ewart, 1982). Moreover, hypermagnesium compositions (Fo_{91-93}) are observed for some Hunter phenocrysts, which have a probable upper mantle origin (Lefèvre et al., in press) and are thus considered as xenocrysts.

Fe-Ti oxides. Opaque minerals are represented by titano-magnetite. Chromiferous spinel, or even chromite (sensu stricto) may occur as inclusions in olivine phenocrysts (Matthew) or xenocrysts (Hunter).

Amphibole. It is worthwhile to note that only one phenocryst of amphibole has been found in some sixty thin-sections of Matthew and Hunter andesites studied. This rare occurrence is a highly pleochroic hornblende, rimmed by opaque minerals, in a pebble fragment of andesite lava from the Matthew southern bay.

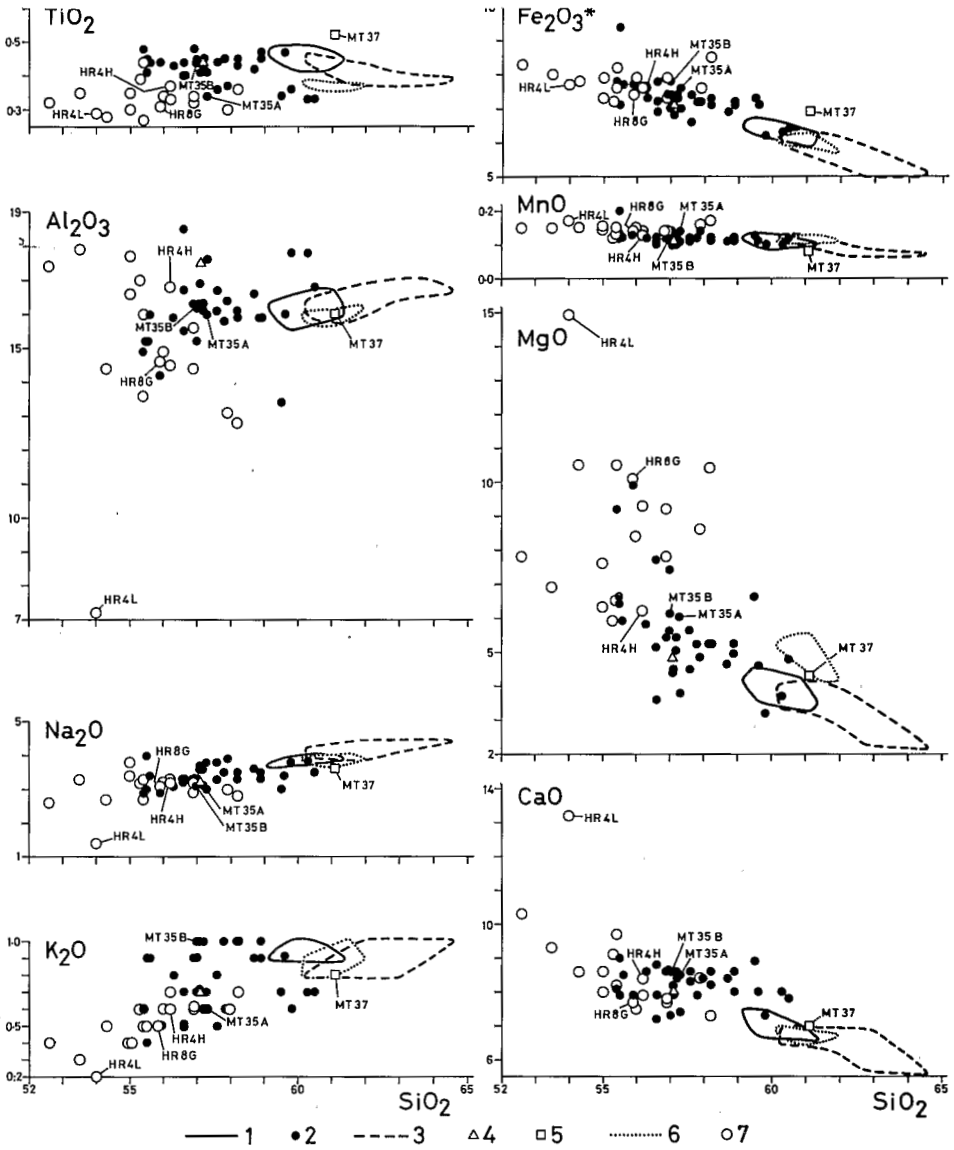

Fig. 7. Major oxides plotted against SiO_2. *1* = East-Matthew lavas; *2* = East-Matthew inclusions; *3* = West-Matthew lavas; *4* = West-Matthew inclusion; *5* = Matthew isthmus inclusion (block MT 37); *6* = Hunter lavas; *7* = Hunter inclusions. Source of data: Tables 1 and 4, and unpublished data. Complete analytical data available upon request (P.M.).

If the general features of the above mineralogy are typical of modern orogenic andesites (Gill, 1981; Ewart, 1982), two peculiarities must be emphasized:

(a) the Hunter olivine xenocrysts are Mg-rich; and (b) hornblende phenocrysts are almost absent in Matthew andesites and completely absent in Hunter lavas.

TABLE 3

Microprobe data of selected minerals in lavas from West-Matthew (MT 24A) and Hunter (HR6)

SAMPLE	MT 24A						HR 6					
MINERAL	PLAG Ph.C.	CPX Ph.C. Endiopside	CPX Ph.R. Augite	OPX Ph.C.	OL Ph.C.	Sp.Cr in OL.	PLAG Ph.C.	CPX Ph.C. Endiopside	CPX Ph.C. Salite	CPX Ph.R. Augite	OPX Ph.C.	OL Ph.C.
SiO_2	53.15	53.83	53.00	55.27	40.50		53.31	52.99	52.82	52.18	53.08	41.33
TiO_2		0.11	0.34	0.23		0.32		0.20	0.21	0.22	0.11	
Al_2O_3	30.42	1.58	1.27	0.93		11.79	29.27	2.71	1.44	1.10	0.87	
Fe_2O_3	0.59					9 48	0 47					
Cr_2O_3		0.75				49.84		0.66				
FeO		4.23	9.20	20.01	11 98	18.28		6.18	8.72	9.64	19.41	7.11
MnO		0.12	0.26	0.46	0.26	0.56		0.18	0.13	0.18	0.41	
MgO		18.07	15.31	24.59	47.12	10.04		17.81	14.49	14.62	24.45	50.78
CaO	12.03	20.70	20.19	1.17	0.18		11.34	19.95	22.54	22.02	1.01	0.08
Na_2O	4.16	0.30	0.33				4.72	0.22	0.26	0 31	0.02	
K_2O	0.13						0.13					
NiO					0.15							0.50
TOTAL	100.48	99.69	99.90	102.66	100.19	100.31	99.24	100.90	100.61	100.27	99.36	99.80
Si	2.393	1.961	1.967	1.977	0.999		2.424	1.922	1.956	1.949	1.966	1.005
Ti		0.003	0.009	0.006		0.063		0.005	0.006	0.006	0.003	
Al	1.612	0.068	0.055	0.039		3.646	1.569	0.116	0.063	0.048	0.038	
Fe3+	0 020					1.871	0.018					
Cr		0.022				10.330		0.019				
Fe^{2+}		0.128	0.285	0.596	0.246	4.009		0.187	0.269	0.300	0.601	0.145
Mn		0.004	0.008	0.014	0.005	0.124		0.006	0.004	0.006	0.013	
Mg		0.988	0.853	1.319	1.743	3.923		0.969	0.805	0.819	1.350	1.840
Ca	0.581	0.808	0.803	0.045	0.005		0.552	0.775	0.894	0.881	0.040	0 002
Na	0.362	0.021	0.024				0.416	0.016	0.019	0.022	0.002	
K	0.008						0.008					
Ni					0.003							0.010
An/An+Ab+Or	61.1						56.6					
$Mg/Mg+Fe^{2+}+Mn$		88.2	74.4	68.4	87.4			83.4	74.7	72.8	68.7	92.7

Analyst: C. Lefèvre. Data from Lefèvre et al. (in press). Camebax microprobe, Université de Paris-Sud, Orsay, France. Analytical procedure: 15 kV, 12 nA, 10 s.
PLAG = plagioclase; CPX = clinopyroxene; OPX = orthopyroxene; OL = olivine; Cr.Sp = = Cr-spinel; Ph = phenocryst; C = core; R = rim. Structural formulae based on 8 oxygens for PLAG, 6 oxygens for CPX and OPX, 4 oxygens for OL, and 32 oxygens for Cr.Sp.

The inclusions

The presence of inclusions in orogenic andesites is a well-known characteristic of these rocks (e.g. Powell, 1978; Arculus and Wills, 1980; Gill, 1981; Conrad et al., 1983; Morrice et al., 1983). However, Matthew and Hunter are the only volcanoes of the New Hebrides island arc where host-lavas contain as many as 1—2% (by volume) of inclusions of various kinds. Besides obvious cumulate-type inclusions (pyroxene- and gabbroic cumulates), apparently restricted to Hunter volcano, doleritic cognate inclusions are widely scattered in volcanics of both islands. In the field, all of them appear as round- or oval-shaped spots, 1—30 cm in diameter, with well-defined limits. They generally contrast with the host-lava in colour, degree of crystallinity, and vesicularity. Because of their greater resistance to weathering, these inclusions give a distinctly patchy appearance to Matthew and Hunter andesites.

TABLE 4

Major- and trace-element analyses of selected inclusions from Matthew and Hunter

	EAST-MATTHEW (= OLD MATTHEW)		MATTHEW (ISTHMUS)	HUNTER				
	DOLERITIC COGNATE		INCLUSIONS	PYROXENE CUMULATE	GABBROIC CUMULATES		DOLERITIC COGNATE INCLUSIONS	
	MT 35A	MT 35B	MT 37	HR 4L	HR 4H	HR 8B	HR 4M	HR 8G
SiO_2	57.3	57.0	61.1	54.0	56.2	55.0	54.3	55.9
TiO_2	0.34	0.44	0.52	0.29	0.37	0.30	0.28	0.31
Al_2O_3	16.0	16.2	16.0	7.2	16.8	16.6	14.4	14.6
Fe_2O_3*	7.6	7.8	6.9	7.7	7.6	7.9	7.8	7.4
MnO	0.14	0.12	0.08	0.17	0.13	0.15	0.15	0.14
MgO	6.0	6.1	4.3	14.9	6.2	7.6	10.5	10.1
CaO	8.5	8.6	7.0	13.2	8.4	8.6	8.6	7.7
Na_2O	3.0	3.1	3.6	1.4	3.2	3.4	2.7	3.1
K_2O	0.6	1.0	0.8	0.2	0.6	0.4	0.5	0.5
LOI	0.0	0.0	0.0	0.2	0.1	0.0	0.6	0.3
TOTAL	99.48	100.36	100.30	99.26	99.60	99.95	99.83	100.05
FeO	5.1	4.6	3.6	6.0	5.3	5.6	5.9	5.5
P_2O_5 CAESS				0.09	0.12	0.12		0.11
Rb CAESS				5	6	5		10
P.SUE	6.1	8.4	9.4					
Sr CAESS				94	470	464		298
P.SUE	379	1058	457					
Ba P.SUE	85	136	111	18	55			81
Zr CAESS				19	52	31		47
Y CAESS				7	10	7		8
Nb CAESS				9	<10	9		16
Th P.SUE	0.69	2.13	1.07	0.09	0.36			0.51
U P.SUE	0.32	0.60	0.52		0.50			
La P.SUE	6.5	16.6	8.1	1.7	4.0			3.8
Ce P.SUE	10.5	38.1	17.8	8.3	13.0			9.6
Sm P.SUE	2.04	3.48	2.44	1.18	1.54			1.26
Eu P.SUE	0.86	1.42	0.84	1.17	1.08			1.29
Tb P.SUE	0.24	0.33	0.33	0.16	0.20			0.17
Yb P.SUE	0.72	1.07	0.90	1.02				0.74
Lu P.SUE	0.19	0.18	0.18	0.13	0.17			0.19
Ni CAESS				231	57	93		173
P.SUE	57	41	48	232	69			218
Cr CAESS				936	163	288		541
P.SUE	213	133	146	731	184			538
V CAESS				221	186	173		160
Sc P.SUE	26.8	25.2	21.3	69.2	25.7			26.6
Sb P.SUE					0.05			0.13
Zn P.SUE					96			

Source of data and analytical procedures: see Table 1.

The pyroxene cumulate (HR 4L; Table 5). This ovoid, up to 30 cm-long, greenish and coarse-grained inclusion contains two types of pyroxene, which appear green or brown in hand-specimen. Cumulus and intercumulus textures can be clearly distinguished in thin-section. The granoblastic cumulus is made up of abundant endiopside (sometimes rimmed by salite), frequent orthopyroxene (Fs_{23-28}) and Mg-olivine (Fo_{82}), rare bytownite, titanomagnetite, and Cr-spinel inclusions in the endiopside. No foliation can be discerned in thin-section. The distinctly vesicular intercumulus contains numerous plagioclase microlites (An_{53-50}), with a typical chilled habit. Augite microlites and orthopyroxene microlites (Fs_{28-30}) are significantly rarer, and opaque grains, exceptional.

P—T conditions calculated from these mineralogical data suggest a ca. 10kbar/1070°C equilibrium, which corresponds to a deep crystallization level (Lefèvre et al., 1982; Lefèvre et al., in press).

TABLE 5

Microprobe data of selected minerals in inclusions from Hunter

SAMPLE	HR 4L PYROXENE CUMULATE					HR 8B GABBROIC CUMULATE			HR 4M DOLERITIC COGNATE INCLUSION			
MINERAL	PLAG cumulus	PLAG inter-cumulus	CPX cumulus endiopside	CPX inter-cumulus augite	OL cumulus	PLAG cumulus	PLAG inter-cumulus	CPX cumulus augite	PLAG Ph.C.	PLAG Ph.R.	PLAG Microph.	OL Ph.C.
SiO_2	49.42	55.69	54.13	52.91	39.84	52.08	55.34	52.51	48.72	53.01	59.23	41.18
TiO_2			0.07	0.49				0.31				
Al_2O_3	31.20	27.07	2.02	2.30		29.71	26.23	1.60	32.09	29.20	24.01	
Fe_2O_3	0.57	1.11				0.71	0.94		0.73	1.01	0.89	
Cr_2O_3			0.37	0.13				0.07				
FeO			5.22	6.81	16.69			9.36				11.29
MnO			0.08	0.22	0.26			0.23				0.19
MgO			16.61	15.71	42.82	0.07	0.12	14.93				47.66
CaO	15.83	11.00	22.11	21.31	0.19	12.22	9.27	20.64	16.39	12.91	7.07	0.15
Na_2O	2.79	5.19	0.28	0.31		3.79	5.79	0.43	2.21	4.21	7.46	
K_2O	0.12	0.34				0.15	0.44		0.12	0.31	0.94	
NiO					0.32							0.22
TOTAL	99.93	100.40	100.89	100.19	100.12	98.73	98.13	100.08	100.26	100.65	99.60	100.69
Si	2.268	2.511	1.961	1.944	1.004	2.390	2.546	1.955	2.232	2.399	2.674	1.005
Ti			0.022	0.013	0.001			0.008				
Al	1.685	1.436	0.086	0.099		1.607	1.423	0.070	1.729	1.554	1.275	
Fe^{3+}	0.020	0.038				0.027	0.036		0.025	0.034	0.030	
Cr			0.011	0.004				0.002				
Fe^{2+}			0.157	0.209	0.351			0.291				0.230
Mn			0.003	0.007	0.006			0.007				0.004
Mg			0.902	0.866	1.622	0.005	0.008	0.828				1.745
Ca	0.779	0.532	0.858	0.839	0.005	0.601	0.457	0.823	0.804	0.626	0.342	0.004
Na	0.248	0.453	0.019	0.022		0.338	0.517	0.031	0.196	0.369	0.652	
K	0.007	0.020				0.009	0.026		0.007	0.018	0.054	
Ni					0.007							0.004
An/An+Ab+Or	75.4	53.0				63.4	45.7		79.9	61.9	32.7	
Mg/Mg+Fe^{2+}+Mn			84.9	80.0	82.0			73.5				88.2

Source of data and analytical procedures: see Table 3.
Microph. = microphenocryst.

The gabbroic cumulates (HR 4H, HR 8B; Table 5). Numerous examples of gabbroic cumulate inclusions can be found in the northern Hunter lava flow. In thin-section, they display sharp borders with the host-lava, and are characterized by a coarse intersertal texture and a high cumulus crystal content (70—90% in vol.). Plagioclase laths (50—60% in vol.) systematically contain abundant fluid inclusions located along cleavage and twinning planes. Moreover, these feldspars (An_{64-45}) usually display a lobate, indented or jagged habit, which may indicate some resorption. Clinopyroxene (augite) and orthopyroxene (Fs_{26-32}) phenocrysts, which may include Fe-Ti oxides, represent the two other main mineral phases. Microphenocrysts are essentially represented by aggregates of highly fragmented pyroxene. Their numerous Fe-Ti oxide inclusions may indicate that they are almost completely resorbed olivine crystals. Olivine can be found, unaltered, in the midst of some of the aggregates. Scarce vesicle-rich glass occurs in interstices and contains plagioclase microlites. Tridymite often crystallizes within the vesicles in the glass.

P—T conditions calculated from these mineralogical data indicate a ca. 3 kbar/1000°C equilibrium. This indicates a shallow (10—12 km) crystallization level (Lefèvre et al., 1982; Lefèvre et al., in press).

The doleritic cognate inclusions (MT 35A, MT 35B, MT 37, HR 4M, HR 8G; Table 5). These inclusions seem to be distributed uniformly within Matthew as well as Hunter andesites. They display a well-defined doleritic texture, though their grain-size can vary highly from one inclusion to another.

Microphenocrysts make up the bulk of the inclusions. Phenocrysts in the inclusions are generally less abundant than in the host-lavas. A small amount of glassy matrix occurs in the groundmass of these inclusions.

The more calcic composition of plagioclase (An_{80-50}) in the inclusions is the only significant chemical difference between host-lava and inclusion phenocrysts. In other words, the habit and composition of clinopyroxene (endiopside-augite), orthopyroxene (Fs_{23-33}), titanomagnetite and olivine (Fo_{84-87}) phenocrysts in these doleritic inclusions are almost identical with that found in the host-lavas. However, their relative proportions differ. Plagioclase and titanomagnetite are less abundant, clinopyroxene more distinctly predominates over orthopyroxene, and olivine is more common in the inclusions.

Microphenocrysts are predominantly plagioclase; augite is subordinate. The microphenocryst feldspars (An_{45-27}) are significantly more sodic than the phenocryst feldspars, and are cemented by a glassy and vesicle-rich matrix, which may indicate that the inclusions were quenched, as noted by Morrice et al. (1983) for some similar inclusions in Indonesia volcanics.

Geochemistry

Major elements

An evaluation of major-element analyses of Matthew and Hunter andesites (Tables 1 and 2) leads to the following observations. Available data are statistically significant for each magmatic suite; the standard deviation for each oxide in the 3 sets of data (East-Matthew, West-Matthew, Hunter) remains distinctly low compared to the corresponding oxide mean value. In fact, obvious chemical similarities appear between Matthew and Hunter volcanics, besides some slight discrepancies, which can be unambiguously related to modal mineral variations (see, for example, the higher MgO content in Hunter andesites, which reflects the higher olivine content in these rocks).

The TiO_2 content of Matthew and Hunter volcanics, among the lowest ones ever recorded in acid orogenic andesites, may indicate a newly established subduction (Gill, 1981) and/or an early fractionation of titanomagnetite (see above). This latter interpretation is compatible with the fact that no inflection appears in the TiO_2 vs. SiO_2 diagram (Fig. 7), since TiO_2 contents regularly decrease (Matthew) or stay stable (Hunter) with increasing SiO_2.

Though strongly plagioclase-phyric, Matthew and Hunter andesites do not show very high Al_2O_3 content (always $\leqslant$ 17%). However, because these

lavas are quite differentiated, their parental magma presumably has already undergone plagioclase fractionation, thus progressively reducing the Al_2O_3 content of the successive residual liquids.

Using SiO_2 as a differentiation index, we have plotted the analyses of Matthew and Hunter inclusions and lavas (Tables 1 and 4) on Harker-type diagrams (Fig. 7). Interestingly, no chemical gap occurs along the whole silica range, and, moreover, the different fields partly overlap. However, two significant patterns appear:

(a) Na_2O vs. SiO_2, on one hand, Fe_2O_3*, MnO and CaO vs. SiO_2 diagrams, on the other, show a rather linear trend for host-lavas as well as for inclusions. This is a strong argument favoring a genetic relationship between them.

(b) By contrast, Al_2O_3 and MgO vs. SiO_2 diagrams display a more complex pattern, resulting from the larger scatter of aluminum and magnesium contents in the inclusions. Nevertheless, on Hunter island, the gabbroic cumulates (e.g. HR 4H) show a distinctly higher Al_2O_3 content and a lower MgO content than the doleritic cognate inclusions (e.g. HR 8G), thus clearly reflecting their respective modal mineralogy.

Trace elements

The preceding paragraph has shown that Matthew and Hunter volcanics do not significantly differ for major-element geochemistry. However, trace-element data, though quantitatively limited, clearly show three distinct groups among the lavas (Table 1).

The Hunter andesitic suite is little fractionated, with high transition element contents (Ni = 36—89 ppm; Cr = 118—236 ppm), and, correspondingly low incompatible element contents (Sr, Th, U, light REE), compared with both East-Matthew and West-Matthew suites. Among the Matthew volcanics, the younger ones (historic West-Matthew andesites) are depleted in incompatible elements relative to the older ones (East-Matthew suite). Cr contents in lavas have been plotted against Th, Sr and La contents in Fig. 8. Trace-element data corresponding to the different kinds of inclusions described above (Table 4) also appear on this figure, for comparison. Since no straight line can be drawn between the three volcanic groups (East-Matthew, West-Matthew, Hunter), mixing can not be invoked for the genesis of any of these suites (Gill, 1981). Instead, a broadly parabolic trend encompasses most of the data, as schematically shown on Fig. 8.

Interestingly, inclusions as well as lavas can be grouped in the same general spectrum, which may indicate either fractional crystallization or batch melting from a common source. The same elements plotted along logarithmic coordinates (Fig. 8) tend to favor the first hypothesis (fractional crystallization), since most analytical points define a nearly linear trend with a steep slope (Gill, 1981). The Ni vs. Cr diagram (Fig. 9) illustrates this conclusion. Note that all doleritic cognate inclusions but one (HR 8G) plot within the lava field. On the other hand, the pyroxene cumulate

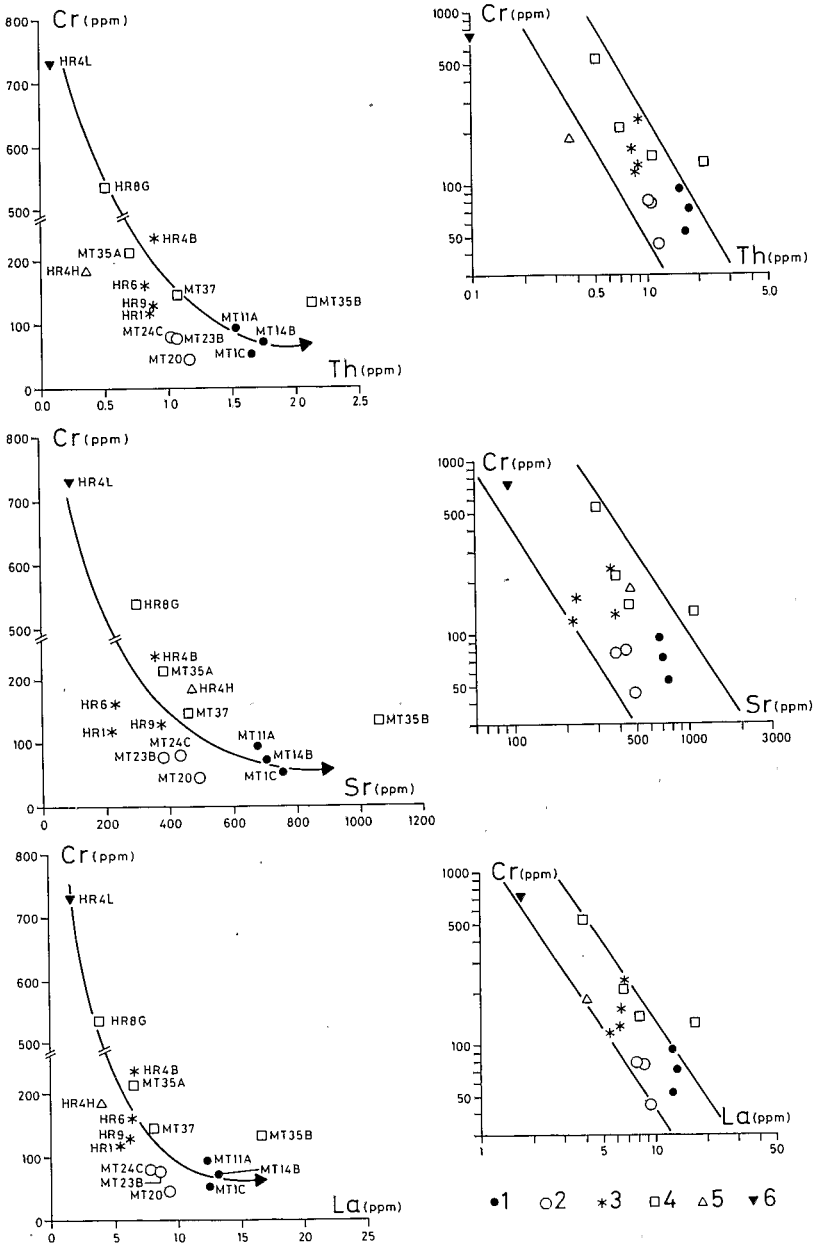

Fig. 8. Rectilinear (left) and logarithmic (right) variation diagrams plotting a compatible element (Cr) versus the incompatible elements Th, Sr, and La. 1 = East-Matthew lavas; 2 = West-Matthew lavas; 3 = Hunter lavas; 4 = doleritic cognate inclusions; 5 = gabbroic cumulate; 6 = pyroxene cumulate. Source of data: Tables 1 and 4.

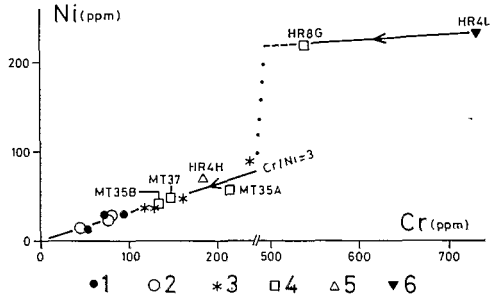

Fig. 9. Rectilinear Ni vs. Cr variation diagram. Same symbols as in Fig. 8. Source of data: Tables 1 and 4. As pointed out by Gill (1981), a fractional crystallization process may explain the trend of the data plotted along the Cr/Ni = 3 line.

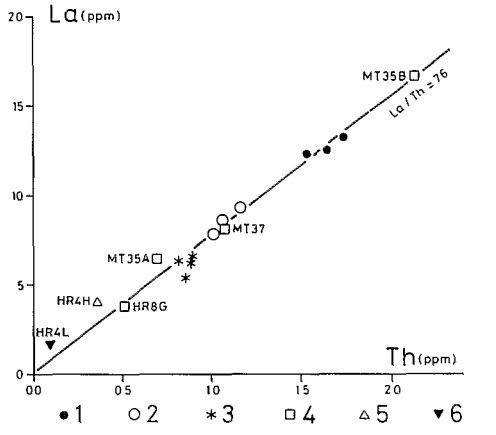

Fig. 10. Rectilinear La vs. Th variation diagram. Same symbols as in Fig. 8. Source of data: Tables 1 and 4.

(HR 4L) presumably represents a primitive, mantle-derived phase, and the doleritic cognate inclusion HR 8G an intermediate product leading to Matthew-Hunter volcanics through early olivine fractionation.

Moreover, a plot of two hygromagmatophile elements with a different degree of incompatibility, such as La and Th, supports this conclusion (Fig. 10). The fact that all analytical points (lavas and inclusions) plot along a straight line intersecting the coordinate origin in such a diagram is a necessary and sufficient condition for proving a differentiation process through fractional crystallization (Treuil and Varet, 1973; Treuil and Joron, 1975). Thus East-Matthew, West-Matthew, and Hunter andesites most likely correspond to fractionates originated from batches of similar 'parental' magmas (Presnall, 1979) with a constant La/Th ratio of ca. 7.6.

REE patterns and modelling. To further testing our conclusion of differentiation via fractional crystallization, we have plotted the chondrite-normalized rare-earth element (REE) data for lavas and inclusions (Fig. 11).

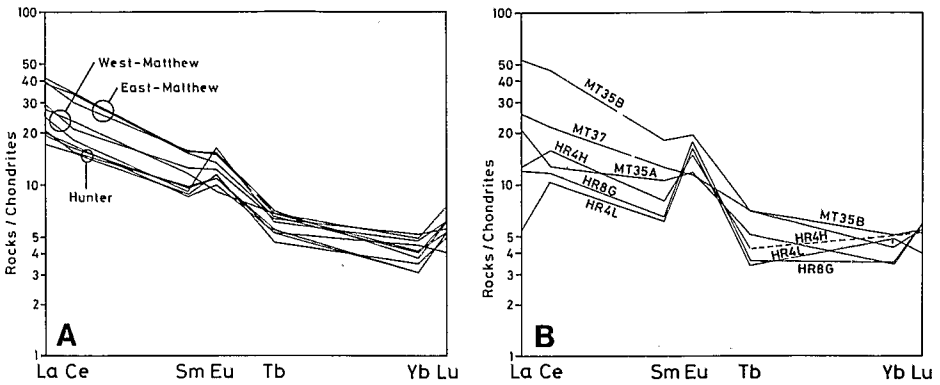

Fig. 11. Chondrite - normalized REE patterns of Matthew-Hunter andesites. A. Lavas. B. Inclusions. Source of data: Tables 1 and 4. Normalizing values: REE values for Leedey chondrite (Masuda et al., 1973) divided by 1.20, except for Tb (from Haskin and Paster, 1979).

Lavas (Fig. 11A). The three volcanic series show distinctly light-REE enriched patterns, with a significant positive Eu anomaly, a depletion in heavy REE from Tb to Yb, and an enrichment in Lu compared with Yb. The light-REE enrichment increases from Hunter through West-Matthew to East-Matthew lavas. While there is no apparent correlation between this light-REE enrichment and the whole-rock silica content, the positive Eu anomaly tends to decrease along with the light-REE enrichment. However, note that, if only one sample (MT 23B) shows a negative Eu anomaly, the highest positive Eu anomaly in sample MT 24C may be related to the high modal plagioclase content (28.1%, Table 1) of the corresponding lava.

Inclusions (Fig. 11B). The REE patterns of inclusions are much more varied, though some of them (e.g. MT 37) closely resemble lava patterns.

REE modelling. Using the mineral-liquid distribution coefficients of Table 6, we have tried to model the behavior of REE during partial fusion and fractional crystallization (Fig. 12). We assume a source material (curve S) which is a garnet peridotite with a two-time chondritic normalized-REE pattern and the following modal composition: olivine (60%), orthopyroxene (20%), clinopyroxene (19.5%) and garnet (0.5%). Small amounts of partial fusion of such a source would induce a strong light-REE enrichment in the liquid formed, as well as comparatively moderate enrichment in heavy-REE (due to the small amount of garnet in the source). Calculations using the batch-melting equation (Gast, 1968) applied to such a starting material show that 6% of modal melting lead to the liquid composition 'PM' (Fig. 12). This 'PM' composition (PM = 'parental magma') is close to the REE compositions of the Hunter andesites (Table 6 and Fig. 11A), except for

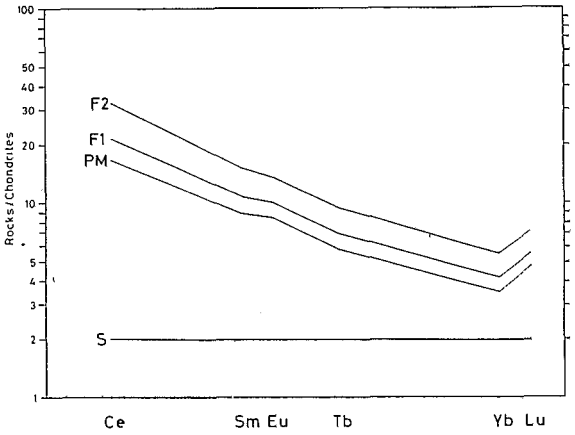

Fig. 12. Interpretation of the chondrite-normalized REE patterns of Matthew-Hunter volcanics. REE modelling (chondrite-normalized patterns) and petrogenetic processes. Partial fusion: 6% of modal melting of a 2-time chondritic garnet peridotite S ("source"): olivine: 60; orthopyroxene: 20; clinopyroxene: 19.5; garnet: 0.5. The REE composition of the liquid obtained with the batch melting equation is shown by the curve PM ('parental magma').
Fractional crystallization: Curves F1 and F2 correspond to 26% and 55%, respectively, of crystallization of PM, using the Rayleigh fractionation equation. The crystallizing phases and their relative proportions are: plagioclase: 25; clinopyroxene: 35; orthopyroxene: 20; olivine: 17; magnetite: 3. The K_D's used in calculations and the REE compositions of S, PM, F1 and F2 are given in Table 6. See text for discussion, and Fig. 11A for comparison.

Eu, whose abundance is slightly lower in the calculated model (PM) than in Hunter andesites (see below). Disregarding this discrepancy, we have used the Rayleigh fractionation equation to model the REE during fractional crystallization of such a parental magma, assuming the following crystallizing phases: plagioclase (25%); clinopyroxene (35%); orthopyroxene (20%); olivine (17%) and magnetite (3%). The models obtained (F1 and F2, in Table 6 and Fig. 12) are in relatively good agreement with the REE patterns of West-Matthew and East-Matthew series, respectively.

However, this modelling does not fully account for the distinctive positive Eu anomaly observed in the three series. In spite of a relative uncertainty concerning the values of the mineral/liquid partition coefficients in andesitic melts, we believe this difference between the model and the observed patterns to be significant. Therefore, if Hunter and Matthew andesites may originate from batches of similar parental magmas by a simple fractional crystallization process, we still have to suppose that their parental melts have been enriched in europium. The origin of such an Eu enrichment remains unclear.

TABLE 6

REE modelling (chondrite-normalized values) compared to Matthew-Hunter REE contents (top). Mineral/liquid partition coefficients (K_D's) used for REE modelling (bottom)

	Ce	Sm	Eu	Tb	Yb	Lu
S	2	2	2	2	2	2
PM	16.53	8.77	8.25	5.74	3.45	4.72
HR	15.25	8.54	9.97	4.68	3.08	4.02
	16.85	9.74	11.36	5.53	4.47	5.26
F1	21.32	10.76	9.91	6.90	4.10	5.53
W-MT	18.08	9.11	9.14	6.17	4.13	5.26
	23.12	12.50	16.34	6.81	5.19	6.19
F2	32.45	15.09	13.42	9.37	5.44	7.17
E-MT	30.01	15.21	13.43	6.60	3.75	6.19
	34.19	15.83	15.51	7.02	4.90	7.43

	PLAG	CPX	OPX	OL	MAGN	GAR
Ce	0.20	0.25	0.05	0.01	0.20	0.028**
Sm	0.11	0.75	0.10	0.01	0.30	1.3
Eu	0.31	0.80	0.12	0.01	0.25	1.6
Tb	0.08*	0.85*	0.30*	0.01*	0.25*	15*
Yb	0.05	0.90	0.46	0.01	0.25	56
Lu	0.04*	0.90*	0.70*	0.02*	0.25*	11.9**

S = source material (garnet peridotite); PM = parental magma (6% of modal melting of S); HR = range of REE contents in Hunter andesites; F1 = fractionate (26% of crystallization of PM; W-MT = range of REE contents in West-Matthew andesites; F2 = fractionate (55% of crystallization of PM); E-MT = range of REE contents in East-Matthew andesites. See text and Fig. 12 for discussion.
PLAG = plagioclase; CPX = clinopyroxene; OPX = orthopyroxene; OL = olivine; MAGN = magnetite; GAR = garnet. Source of data: Gill, 1981; Arth, 1976 (**). * = estimated value.

DISCUSSION AND CONCLUDING REMARKS

Our study has shown that, besides some evident petrographic resemblances, the andesites from Matthew and Hunter correspond to three distinct, but genetically related volcanic suites, i.e. the Hunter, East-Matthew and West-Matthew groups. Despite the lack of radiometric as well as isotopic data for constraining more strongly any interpretation, the following proposed scheme may satisfactorily account for most of the observations.

Both volcanoes are the products of successive batches of similar parental magmas, originated by limited degrees of partial fusion of a garnet peridotite. The most probable source for such a fusion onset lies in the mantle wedge overlying the subducting slab.

The little-fractionated Hunter andesites are directly derived from the crystallization of one batch of these parental magmas. On the other hand, the genesis of the Matthew volcanics has been marked by various degrees of fractional crystallization. This process clearly does not correlate with the eruptive chronology of the volcano, since the older edifice (East-Matthew) is significantly more evolved than the younger (historic) one (West-

Matthew). It is thus probable that successive refilling of magmatic chambers below the volcano allows a variable evolution of the melt, depending on still unconstrained thermodynamic conditions. However, the petrological study of the Matthew andesites emphasizes this paradoxical observation: if the West-Matthew lavas (the younger ones) including the recent northwestern lava flow, are richer in plagioclase phenocrysts and more evolved, based on major-element criteria, than the East-Matthew group, the former ones also underwent a lesser amount of fractional crystallization judging from their trace and rare-earth element data.

Therefore, this study emphasizes the importance of the internal evolution of successive batches of similar parental magmas, which may lead to little-fractionated volcanics (Hunter), together with ancient and fractionated lavas (East-Matthew), as well as more recent and less-fractionated products (West-Matthew). The genetic relationship between the Matthew-Hunter andesites and their inclusions are discussed elsewhere (Lefèvre et al., in press). However, the geodynamic connection between the southern New Hebrides arc and the North Fiji Basin remains to be addressed. Standing halfway from an intraoceanic collision zone (Loyalty Islands Ridge vs. New Hebrides arc) and an active expanding ridge (North Fiji Basin Ridge), the Matthew and Hunter volcanoes most likely reflect in their petrological evolution the combined influence of both phenomena.

ACKNOWLEDGEMENTS

We are greatly indebted to the following individuals and institutions which made this research possible: the R/V "VAUBAN" (ORSTOM-Nouméa), her captain (P. Furic) and crew; the French Navy (TCD "OURAGAN"), the French Air Force (Puma helicopters) and the Aéronavale-Tontouta (Neptune P2H aircraft); the SHOM-MOP (Service Hydrographique et Océanographique de la Marine — Mission océanographique du Pacifique). C. Vacquier (ORSTOM-Nouméa) and H. Martin (CAESS, Université de Rennes, France) greatly helped us for the computer analysis of our data. J.B. Gill, P. Whelan and UCSC (University of California Santa Cruz) faculty, staff and students made the one-year-long stay of one of us (PM) in Santa Cruz nice and profitable. We would like also to thank D. Duhet and S. Le Corvaisier (ORSTOM-Nouméa: major-element analyses), F. Vidal (CAESS, Université de Rennes: trace-element analyses), G. Meyer (Groupe des Sciences de la Terre, Laboratoire P. Sue, CEN Saclay, France: trace-element and REE analyses), H. Joly and J. Le Gat (typing), J. Butscher (drafting) and P. Ribere (photographs), for their essential contribution to this paper.

Early versions of this paper were reviewed by Patricia Fryer and Loren Kroenke (Hawaii Institute of Geophysics), and by two anonymous reviewers, who are thanked for their constructive comments.

Last but not least, J. Recy (Head of the Geology-Geophysics Department,

ORSTOM-Nouméa) gave us the opportunity as well as the financial and intellectual liberty to undertake this research.

REFERENCES

Arculus, R.J. and Wills, K.J.A., 1980. The petrology of igneous plutonic blocks and inclusions from the Lesser Antilles island arc. J. Petrol., 21: 743—799.

Arculus, R.J., 1981. Island arc magmatism in relation to the evolution of the crust and mantle. In: R.E. Zartman and S.R. Taylor (Editors), Evolution of the Upper Mantle. Tectonophysics, 75: 113—133.

Arth, J.G., 1976. Behavior of trace elements during magmatic processes. A summary of theoretical models and their applications. J. Res., U.S. Geol. Surv., 4(1): 41—47.

Barsdell, M., Smith, I.E.M. and Sporli, K.B., 1982. The origin of reversed geochemical zoning in the northern New Hebrides volcanic arc. Contrib. Mineral. Petrol., 81: 148—155.

Beck, Jr., M.E., 1983. On the mechanism of tectonic transport in zones of oblique subduction. Tectonophysics, 93: 1—11.

Blot, C., 1976. Volcanisme et sismicité dans les arc insulaires. Prévision de ces phénomènes. ORSTOM, Géophysique, 13, 206 pp.

Briqueu, L. and Lancelot, J.R., 1983. Sr isotopes and K, Rb, Sr balance in sediments and igneous rocks from the subducted plate of the Vanuatu (New Hebrides) active margin. Geochim. Cosmochim. Acta, 47: 191—200.

Carney, J.N. and Macfarlane, A., 1982. Geological evidence bearing on the Miocene to recent structural evolution of the New Hebrides arc. In: G.H. Packham (Editor), The Evolution of the India—Pacific Plate Boundaries. Tectonophysics, 87: 147—175.

Collot, J.Y., Daniel, J. and Burne, R.V., 1985. Recent tectonics associated with the subduction/collision of the D'Entrecasteaux Zone in the central New Hebrides. Tectonophysics, 112: 325—356.

Conrad, W.K., Kay, S.M. and Kay, R.W., 1983. Magma mixing in the Aleutian arc: evidence from cognate inclusions and composite xenoliths. In: S. Aramaki and I. Kushiro (Editors), Arc Volcanism. J. Volcanol. Geotherm. Res., 18: 279—295.

Coudert, E., Isacks, B.L., Barazangi, M., Louat, R., Cardwell, R., Chen, A., Dubois, J., Latham, G. and Pontoise, B., 1981. Spatial distribution and mechanisms of earthquakes in the southern New Hebrides arc from a temporary land and ocean bottom seismic network and from worldwide observations. J. Geophys. Res., 86: 5905—5925.

Coulon, C. and Maury, R.C., 1981. Petrology of tholeiitic lavas from Tanna island (New Hebrides): importance of cumulative processes in island arc magmatism. Bull. Volcanol., 44: 661—680.

Curtis, R., 1962. Petrographic description of a specimen from Matthew island submitted by R. Priam. N.H. Condom. Geol. Surv., unpubl. report, 2 pp.

Daniel, J., Collot, J.Y., Ibrahim, A.K., Isacks, B.L., Latham, G.V., Louat, R., Maillet, P., Malahoff, A. and Pontoise, B., 1982. La subduction aux Nouvelles-Hébrides. In: Equipe de Géologie-Géophysique du Centre ORSTOM de Nouméa. Contribution à l'étude géodynamique du Sud-Ouest Pacifique. Trav. Doc. l'ORSTOM, 147: 149—156.

Dubois, J., Launay, J., Récy, J. and Marshall, J., 1977. New Hebrides trench: subduction rate from associated lithospheric bulge. Can. J. Earth Sci., 14: 250—255.

Dupuy, C., Dostal, J., Marcelot, G., Bougault, H., Joron, J.L. and Treuil, M., 1982. Geochemistry of basalts from central and southern New Hebrides arc: implication for their source rock composition. Earth Planet. Sci. Lett., 60: 207—225.

Ewart, A., 1976. Mineralogy and chemistry of modern orogenic lavas. Some statistics and implications. Earth Planet. Sci. Lett., 31: 417—432.

Ewart, A., 1982. The mineralogy and petrology of Tertiary—Recent orogenic volcanic rocks: with special reference to the andesite - basaltic compositional range. In: R.S. Thorpe (Editor), Andesites — Orogenic Andesites and Related Rocks. John Wiley, New York, N.Y., pp. 25—95.

Fisher, N.H., 1957. Catalogue of the active volcanoes of the world including solfatara fields. Part V: Melanesia. International Volcanological Association, Naples, pp. 102—105.

Fitch, T.J., 1972. Plate convergence, transcurrent faults, and internal deformation adjacent to southeast Asia and the Western Pacific. J. Geophys. Res., 77: 4432—4460.

Gast, P.W., 1968. Trace element fractionation and the origin of tholeiitic and alkaline magma types. Geochim. Cosmochim. Acta, 32: 1057—1086.

Gill, J.B., 1981. Orogenic Andesites and Plate Tectonics. Springer-Verlag, Berlin, 390 pp.

Gorton, M.P., 1977. The geochemistry and origin of Quaternary volcanism in the New Hebrides. Geochim. Cosmochim. Acta, 41: 1257—1270.

Green, T.H., 1972. Crystallization of calcalkaline andesite under controlled high-pressure hydrous conditions. Contrib. Mineral. Petrol., 34: 150—166.

Halunen, A.J., 1979. Tectonic history of the Fiji plateau. Ph.D. thesis, Univ. Hawaii, 127 pp. (unpubl.).

Haskin, L.A. and Paster, T.P., 1979. Geochemistry and mineralogy of the rare earths. In: K.A. Gschneidner, Jr. and L. Eyring (Editors), Handbook on the Physics and Chemistry of Rare Earths. North Holland Publishing Company, Amsterdam, pp. 1—80.

Isacks, B. and Molnar, P., 1971. Distribution of stresses in the descending lithosphere from a global survey of focal-mechanism solutions of mantle earthquakes. Rev. Geophys. Space Phys., 9: 103—174.

Isacks, B.L., Cardwell, R.K., Chatelain, J.L., Barazangi, M., Marthelot, J.M., Chinn, D. and Louat, R., 1981. Seismicity and tectonics of the central New Hebrides island arc. In: D.W. Simpson and P.G. Richards (Editors), Earthquake Prediction. An International Review. AGU, Washington, D.C., pp. 93—116.

Johnson, T. and Molnar, P., 1972. Focal mechanisms and plate tectonics of the southwest Pacific. J. Geophys. Res., 77: 5000—5032.

Koch, P., 1958. Introduction à la géologie de la Nouvelle-Calédonie et de ses dépendances. Bull. Géol. Nouvelle-Calédonie, 1: 20—21.

Lefèvre, C., Maillet, P. and Monzier, M., 1982. Minéralogie des laves de Hunter (arc insulaire des Nouvelles-Hébrides) et de leurs cumulats. Implications pétrogénétiques. 9ème Réunion Annuelle des Sciences de la Terre, Paris, Soc. Géol. Fr., p. 367.

Lefèvre, C., Maillet, P. et Monzier, M. Minéralogie des andésites et des enclaves des volcans Matthew et Hunter (arc des Nouvelles-Hébrides - Sud-Ouest Pacifique). Bull. Minéral., in press.

Louat, R., 1982. Sismicité et subduction de la terminaison sud de l'arc insulaire des Nouvelles-Hébrides. In: Equipe de Géologie-Géophysique du Centre ORSTOM de Nouméa. Contribution à l'étude géodynamique du Sud-Ouest Pacifique. Trav. Doc. l'ORSTOM, 147: 179—185.

Louat, R., Hamburger, M. and Monzier, M. Shallow- and intermediate-depth seismicity in the New Hebrides island arc: constraints on the subduction process. Am. Assoc. Pet. Geol. Bull., in press.

Maillet, P. and Gill, J.B., 1980. Petrology of Matthew and Hunter volcanoes, New Hebrides. EOS, 61(46): 1140 (abstract).

Maillet, P. and Monzier, M., 1982. Volcanisme et pétrologie des îles Matthew et Hunter: données préliminaires. In: Equipe de Géologie-Géophysique du Centre ORSTOM de Nouméa. Contribution à l'étude géodynamique du Sud-Ouest Pacifique. Trav. Doc. l'ORSTOM, 147: 187—215.

Maillet, P., Monzier, M. and Lefèvre, C., 1982. Pétrologie des volcans Matthew et Hunter, Vanuatu (ex-Nouvelles-Hébrides). 9ème Réunion Annuelle des Sciences de la Terre, Paris, Soc. Géol. Fr., p. 398.

Marcelot, G., Maury, R.C. and Lefèvre, C., 1983. Mineralogy of Erromango lavas (New Hebrides): Evidence of an early stage of fractionation in island arc basalts. Lithos, 16: 135—151.

Masuda, A., Nakamura, N. and Tanaka, T., 1973. Fine structures of mutually normalized rare-earth patterns of chondrites. Geochim. Cosmochim. Acta, 37: 239—248.

Monzier, M., Maillet, P., Foyo Herrera, J., Louat, R., Missègue, F. and Pontoise, B., 1984a. The termination of the southern New Hebrides subduction zone (south-western Pacific). Tectonophysics, 101: 177—184.

Monzier, M., Collot, J.Y. and Daniel, J., 1984b. Carte bathymétrique des parties centrale et méridionale de l'arc insulaire des Nouvelles-Hébrides. ORSTOM Paris.

Morrice, M.G., Jezek, P.A., Gill, J.B., Whitford, D.J. and Monoarfa, M., 1983. An introduction to the Sangihe arc: volcanism accompanying arc-arc collision in the Molucca sea, Indonesia. J. Volcanol. Geotherm. Res., 19: 135—165.

Nesbitt, R.W. and Hamilton, D.L., 1970. Crystallization of an alkali olivine basalt under controlled P_{O_2}–P_{H_2O} conditions. Phys. Earth Planet. Inter., 3: 309—315.

Osborn, E.F., 1962. Reaction series for subalkaline igneous rocks based on different oxygen pressure conditions. Am. Mineral., 47: 211—226.

Pascal, G., Isacks, B.L., Barazangi, M. and Dubois, J., 1978. Precise relocations of earthquakes and seismotectonics of the New Hebrides island arc. J. Geophys. Res., 83: 4957—4973.

Powell, M., 1978. Crystallization conditions of low-pressure cumulate nodules from the Lesser Antilles island arc. Earth Planet. Sci. Lett., 39: 162—172.

Presnall, D.C., 1979. Fractional crystallization and partial fusion. In: H.S. Yoder Jr. (Editor), The Evolution of the Igneous Rocks: Fiftieth Anniversary Perspectives. Princeton University Press, Princeton, N.J., pp. 59—75.

Priam, R., 1962. Rapport préliminaire à propos d'une récente visite à l'îlot Matthew (Sud des Nouvelles-Hébrides). Rapport Service Mines Condom. N.H., 10 pp. Unpubl.

Priam, R., 1964. Contribution à la connaissance du volcan de l'îlot Matthew (Sud des Nouvelles-Hébrides). Bull. Volcanol., 27: 331—339.

Rémy, J.M., 1963. Le volcan de l'île Matthew (Nouvelles-Hébrides). C.R. Acad. Sci. Paris, 257: 198—200.

Roca, J.L., 1978. Contribution à l'étude pétrologique et structurale des Nouvelles-Hébrides. Thesis, Montpellier, 158 pp. (unpubl.).

Simkin, T., Siebert, L., McClelland, L., Bridge, D., Newhall, C. and Latter, J.H., 1981. Volcanoes of the World. Smithsonian Institution, Washington, D.C., 233 pp.

Sykes, L.R., Isacks, B.L. and Oliver, J., 1969. Spatial distribution of deep and shallow earthquakes of small magnitudes in the Fiji-Tonga region. Bull. Seismol. Soc. Am., 59: 1093—1113.

Taylor, G.A., 1956. Review of volcanic activity in the territories of Papua New Guinea, the Solomon and New Hebrides islands (1951—1953). Bull. Volcanol., 18: 36.

Thorpe, R.S. (Editor), 1982. Andesites. Orogenic Andesites and Related Rocks. John Wiley, New York, N.Y., 724 pp.

Treuil, M. and Varet, J., 1973. Critères volcanologiques, pétrologiques et géochimiques de la genèse et de la différenciation des magmas basaltiques: exemple de l'Afar. Bull. Soc. Géol. Fr., (7), XV, 5—6: 506—540.

Treuil, M. and Joron, J.L., 1975. Utilisation des éléments hygromagmatophiles pour la simplification de la modélisation quantitative des processus magmatiques. Exemples de l'Afar et de la dorsale médioatlantique. Soc. Ital. Mineral. Petrol., XXXI (1): 125—174.

Vidale, J. and Kanamori, H., 1983. The October 1980 earthquake sequence near the New Hebrides. Geophys. Res. Lett., 10: 1137—1140.